19 May 1995

ELSEVIER

Chemical Physics Letters 237 (1995) 387–398

CHEMICAL PHYSICS LETTERS

Time-gated photon echo spectroscopy in liquids

P. Vöhringer [1], D.C. Arnett [2], T.-S. Yang, N.F. Scherer [3]

Department of Chemistry, University of Pennsylvania, Philadelphia, PA 19104-6323, USA

Received 20 December 1994; in final form 10 March 1995

Abstract

Optical dephasing of a cyanine dye chromophore in solution is investigated by time-gated photon echo spectroscopy in a three-pulse scattering geometry. The third-order polarization response is gated by up-conversion with a reference pulse in a nonlinear optical crystal. Time gating establishes two controllable periods of system evolution in an optical coherence. The measurements are compared with numerical simulations employing the measured OKE spectrum of solvent (butanol, DMSO) fluctuations. The time-shift of the time-gated echo signals for several grating forming pulse time delays agrees with simulation while the narrower simulated widths suggest a frequency-dependent solute–solvent interaction and the consideration of chromophore vibronic transitions.

1. Introduction

Time and frequency domain experiments on optical dephasing of molecular chromophores in solution [1] are attractive for elucidation of bath fluctuations that are of importance to chemical reaction [2–5] and photophysical processes [6]. Time-domain four-wave mixing (FWM) techniques such as two- and three-pulse photon echo (2PE, 3PE) measurements provide a sensitivity to the range of timescales that govern the time evolution of the impulsively prepared optical coherence state of the chromophore in solution. These studies can provide a comprehensive picture of dynamics in liquids over a wide variety of timescales ranging from a few tens of femtoseconds to several milliseconds. The rapid response is dominated by ultrafast solvent motions [7] while the long-time dynamics are characterized by slow degrees of freedom of the bath resulting in spectral diffusion [8,9]. By contrast, frequency domain (i.e. cw-) linear absorption and emission measurements are non-selective in terms of the timescale on which solvent fluctuations can affect electronic coherence in the chromophore.

Mukamel and co-workers [10–12] have developed the nonlinear response function formalism to describe the decay of solute coherence with correlation function techniques. The treatment of multiple degrees of freedom of the solvent interacting with the chromophore, and the collapse of the solvent N-body dynamics into one or a few degrees of freedom, is achieved through a multimode Brownian oscillator (MBO) picture. This formalism enables describing solute–bath interactions from the homogeneous to inhomogeneous limits through choice of the bath inverse correlation time and magnitude of the fluctuation in the line broadening function [13], but fails in providing physical insight into the nature of the solute–solvent coupling. Shemetulskis and Loring [7] have, through a semiclassical treatment, investi-

[1] Deutsche Forschungsgemeinschaft Postdoctoral Fellow.
[2] Department of Education GAANN Predoctoral Fellow.
[3] National Science Foundation National Young Investigator.

SSDI 0009-2614(95)00362-2

gated the microscopic solvent fluctuations that result in optical dephasing of a model chromophore.

Several notable experimental advances and analysis approaches have begun to elucidate the solvent fluctuations that influence optical dephasing. Weiner et al. [14] measured homogeneous and inhomogeneous limit responses in liquid and static media. Shank and co-workers [15] have shown that chromophore dephasing in liquids is a non-Markovian process. Wiersma and co-workers [16] have used the MBO model to simultaneously analyze a set of experimental results for resorufin in DMSO. Joo and Albrecht [17] have shown that fast (homogeneous) fluctuations and slow (inhomogenous, spectral diffusion) processes can be probed through three-pulse echo spectroscopies. Dephasing in DFWM was argued by Simon and co-workers [18] to occur 'on multiple timescales'. These concepts have been taken further by Wiersma's group to simulate echo responses by a fast (non-Markovian) BO and a slow (Markovian) BO [19]. Recently, Bardeen and Shank [20] considered intra-chromophore modes in photon echo analysis and established that dephasing of polar dye molecules in alcohols scales inversely with alcohol chain length, implying the involvement of -OH motions.

Solvent-dependent studies with 17–20 fs pulses have shown [21,22] that the two-pulse photon echo is sensitive to fluctuations of the surrounding solvent bath that occur in the sub-hundred femtosecond regime; motions that give rise to far-IR and Rayleigh-wing activity below 300 cm^{-1}. This similarity of timescales implies that the results of photon echo studies should be compared with other FWM studies that are also sensitive to observable pure solvent spectral densities, such as IR, Rayleigh or Raman. In particular, we have shown that the correlation function of the chromophore transition frequency of cyanine dyes dissolved in polar solvents is well described by the correlation function of equilibrium fluctuations of the pure solvent [21,22]. The latter is independently obtained through vibrationally impulsive optical Kerr effect experiments. Within the framework of linear response theory, this work demonstrates that it is possible to 'predict' the photon echo response from the polarizability spectral density of the neat liquid and an understanding of the solvent property involved in the solute–solvent coupling. In the case studied, the solvent polarizability was shown to be the physical property dictating the interaction. Nevertheless, *time-integrated* photon echoes contain insufficient information to uniquely establish the correct form for the spectral density for optical dephasing.

Cho and Fleming [23] have recently proposed a unique experimental method to extract details about homogeneous and inhomogeneous broadening contributions to the linewidth of the electronic transition of a chromophore in solution. The technique is a three-beam scattering spectroscopy described at the level of the resonant fifth-order nonlinear optical susceptibility. The essential point of their proposal was to obtain two controllable periods of propagation in an optical coherence to better determine the time for rephasing of the polarization. However, since this approach is described at the level of $\chi^{(5)}$, the nonlinear response function is composed of 16 distinct Liouville space pathways (i.e. Feynman diagrams) and their complex conjugates. Therefore, complete analysis of experimental data requires more possible contributions to the signal than at the level of FWM spectroscopy, $\chi^{(3)}$, and two more nested time integrals and propagation periods.

This Letter presents an alternative approach for the elucidation of the solvent spectral density for chromophore dephasing that gives more direct access to the correlation function describing optical dephasing than time-integrated echo measurements. The central concept of the experiment is the *time-gated* (i.e. time-resolved) detection of the third-order polarization response of the sample as opposed to the 'conventional' time-integrated detection of the photon echo. Time-gating is achieved by way of frequency up-conversion [24–28] of the emitted third-order polarization response in a nonlinear crystal. This approach also obtains two controlled periods of evolution in an optical coherence; one is defined by the first two electric field interactions (t_{12}) and the other by the third field and the gate pulse (t_{3g}). In the case where the bath fluctuations allow a timescale separation, this technique permits unambiguous determination of the homogeneous contribution to the linewidth for a diagonal measurement (i.e. $t_{12} = t_{3g}$) and the inhomogenous contribution through the temporal width of the gated echo. The computational effort involved in simulating time-gated photon echo spectroscopy is even less than that required for time-integrated $\chi^{(3)}(t)$ echoes.

Time-gating of the third-order nonlinear polariza-

tion response has been previously demonstrated by Fayer and co-workers [25] in the study of the photon echo response in low temperature solids. The approach has also recently been applied to degenerate FWM responses in semiconductors [26,27]. Transient grating experiments at interfaces have also benefitted from improved temporal resolution through time-gating of the polarization response in a nonlinear crystal [28]. In this Letter we present the results of the first time-gated three-pulse photon echo measurements of chromophore dephasing in room temperature liquids. The demonstration and analysis is performed for the symmetric cyanine dye molecule 1,1′,3,3,3′,3′-hexamethyl-4,4′,5,5′-dibenzo-2,2′-indotricarbocyanine perchlorate (HDITCP) in two polar solvents.

2. Perspective and theory

The difference between the up-converted photon echo measurement and the conventional two- or three-pulse photon echo can be illustrated by considering the case where a system is excited by two delta-function pulses separated by a delay ($\tau = t_{12}$). In an ordinary photon echo arrangement, the two external fields interact in the material to create a third-order polarization or signal field that propogates in the momentum matched direction $2k_2 - k_1$. This signal field is usually referred to as the photon echo. The two optical pulses and the induced polarization, $P^{(3)}(t')$, for this case are shown schematically in Fig. 1a. The two-pulse photon echo is conventionally detected by integrating over the entire third-order polarization response, shown as the shaded area in Fig. 1a, with a photon-detector. This yields the time-integrated modulus square of the signal field (i.e. polarization) as a function of pulse separation; a process described by Eq. (1) below.

In time-gated photon echo spectroscopy, the *temporal shape* of the signal field (modulus square) is detected as a function of delay between pulses. This process is shown in Fig. 1b. Here, instead of integrating over the entire signal field, a gating pulse provides a measure of the instantaneous polarization intensity at a time t' after the last echo forming pulse. In essence, this measurement traces out the magnitude of $|P^{(3)}(t', \tau)|^2$ in time t' for any given pulse separation τ, as described by Eq. (5) below. The additional time parameter provides significantly more information to establish the spectrum of bath fluctuations causing electronic dephasing than obtainable from the time-integrated photon echo.

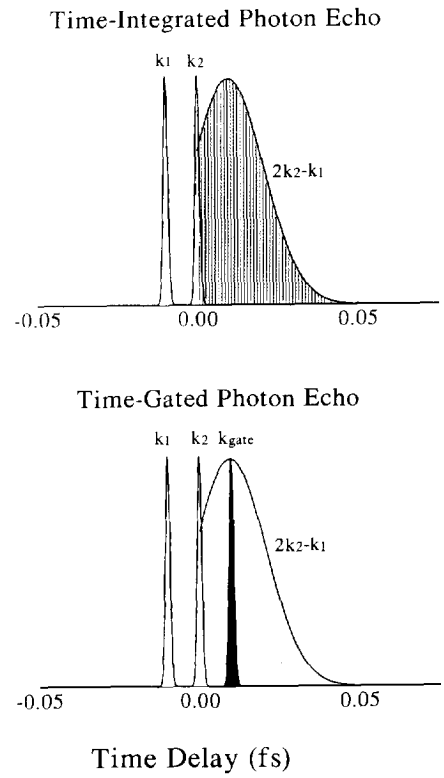

Fig. 1. (a) Schematic of the time-integrated photon echo experiment. The measured signal is the shaded region under the curve of the total polarization response. (b) Time-gated photon echo measurement. The measured signal is illustrated by the portion of the total polarization response overlapped with the third pulse, the gate pulse (solid black).

Experimental photon echo and up-converted photon echo data can be analyzed by comparison with simulated signals obtained using the nonlinear response function description of $P^{(3)}(t_1, t_2, t_3, t)$, spectroscopy [10–12]. In this framework different FWM measurements of the time evolution of a solute–solvent system contain complementary information about the time correlation function of solvent fluctuations. The evolution of electronic phase reflects the form of the chromophore–bath interaction potentials and the correlation time of solvent fluctuations. Information from a variety of measurements can in principle be combined or compared to extract the solute and

solvent frequencies, couplings and relaxation dynamics. The non-linear optical signals can be expressed as a convolution of the appropriate molecular response functions with a sequence of excitation fields.

In FWM processes the pump and probe pulses combine in the sample to create a nonlinear polarization that, in turn, radiates an electric field. In the case of the two-pulse photon echo, the time-integrated signal in the $2k_2 - k_1$ direction is expressed as a function of delay τ between the two pulses as

$$I(\tau) = \int_{-\infty}^{\infty} \mathrm{d}t \, |P^{(3)}_{2k_2-k_1}(t, \tau)|^2. \tag{1}$$

In the rotating wave approximation the third-order polarization is written as

$$\begin{aligned} P^{(3)}_{2k_2-k_1}(t, \tau) = & \int_0^{\infty} \mathrm{d}t_3 \int_0^{\infty} \mathrm{d}t_2 \int_0^{\infty} \mathrm{d}t_1 \{(R_1 + R_4) \\ & \times \exp[-\mathrm{i}\omega_{\mathrm{eg}}(t_3 + t_1)] \exp[-\mathrm{i}\Omega(t - t_3 - t_1 - 2\tau)] \\ & \times E_2(t - t_3 - \tau) E_1^*(t - t_3 - t_2) \\ & \times E_2(t - t_3 - t_2 - t_1 - \tau) + (R_2 + R_3) \times \\ & \exp[-\mathrm{i}\omega_{\mathrm{eg}}(t_3 - t_1)] \exp[-\mathrm{i}\Omega(t - t_3 + t_1 - 2\tau)] \\ & \times E_2(t - t_3 - \tau) E_2(t - t_3 - t_2 - \tau) \\ & \times E_1^*(t - t_3 - t_2 - t_1)\}. \end{aligned} \tag{2}$$

Here $E(t)$ is the temporal profile of the field amplitude, Ω is the laser center frequency, ω_{eg} is the energy difference between excited, $|\mathrm{e}\rangle$, and ground, $|\mathrm{g}\rangle$, electronic states at the equilibrium position (i.e. the 0–0 transition frequency), R_i represents the material response function and an asteriks means complex conjugate. The wavevectors of the pump and probe beams are omitted for simplicity although they are essential in a complete description of signal detection. The molecular response function, $R(t, \tau)$, contains the temporal response of the molecular system for pulses separated in time by τ and is given by combinations of the line broadening functions, $g(t)$. The line broadening function is obtained from the correlation function of the energy difference between the electronic states. Further details of the form of the response functions used here are given elsewhere [11,29].

It was demonstrated that the OKE susceptibility could be used to simulate the time-integrated photon echo signals [21,22]. Therefore, the OKE signal is assumed to describe the spectral density of solvent-induced electronic energy fluctuations, $C_{\mathrm{PE}}(\omega)$. The Wiener–Khintchine theorem and the fluctuation–dissipation theorem can be used to formally make this connection as [11,29]

$$\begin{aligned} C_{\mathrm{PE}}(\omega) &= \int_{-\infty}^{\infty} \mathrm{d}t \, \langle U(t)U(0)\rangle \exp(\mathrm{i}\omega t) \\ &= N\left[1 + \coth\left(\frac{\hbar\omega}{2k_{\mathrm{B}}T}\right)\right] \mathrm{Im}[\chi_{\mathrm{OKE}}(\omega)], \end{aligned} \tag{3}$$

where N is an adjustable parameter reflecting the solute–solvent coupling. The line broadening function representing the spectral density of solvent coupling to solute is given by [11,12]

$$\begin{aligned} g(t) = & \frac{1}{2\pi} \int_{-\infty}^{\infty} \mathrm{d}\omega \frac{1 - \cos(\omega t)}{\omega^2} C(\omega) \\ & + \frac{\mathrm{i}}{2\pi} \int_{-\infty}^{\infty} \mathrm{d}\omega \frac{\sin(\omega t) - \omega t}{\omega^2} C(\omega) + \mathrm{i}\lambda t. \end{aligned} \tag{4}$$

Here, λ is the Stokes-shift and ω is the frequency variable parameterizing the solvent oscillators.

Finally, the up-converted echo signal is experimentally generated with a gate pulse in a nonlinear crystal and detected as the second harmonic intensity. The integrated intensity of the second harmonic signal is written as

$$I(t', \tau) = \int_{-\infty}^{\infty} \mathrm{d}t \, |P^{(3)}(t, \tau)|^2 \, |E_{\mathrm{g}}(t - t' - \tau)|^2, \tag{5}$$

where $|E_{\mathrm{g}}(t)|^2$ is the intensity profile of the gating pulse. As compared with Eq. (1), two adjustable time delays define the complete profile of the echo response. In the results presented below, the duration of the gating pulse is less than the polarization response thereby allowing the temporal profile of the polarization response to be resolved.

A continuous spectrum of solvent modes is assumed and generated by interpolation of experimental data. The details of the Monte Carlo numerical integration method used to evaluate the signals represented in Eqs. (1) and (5) and further development of the associa-

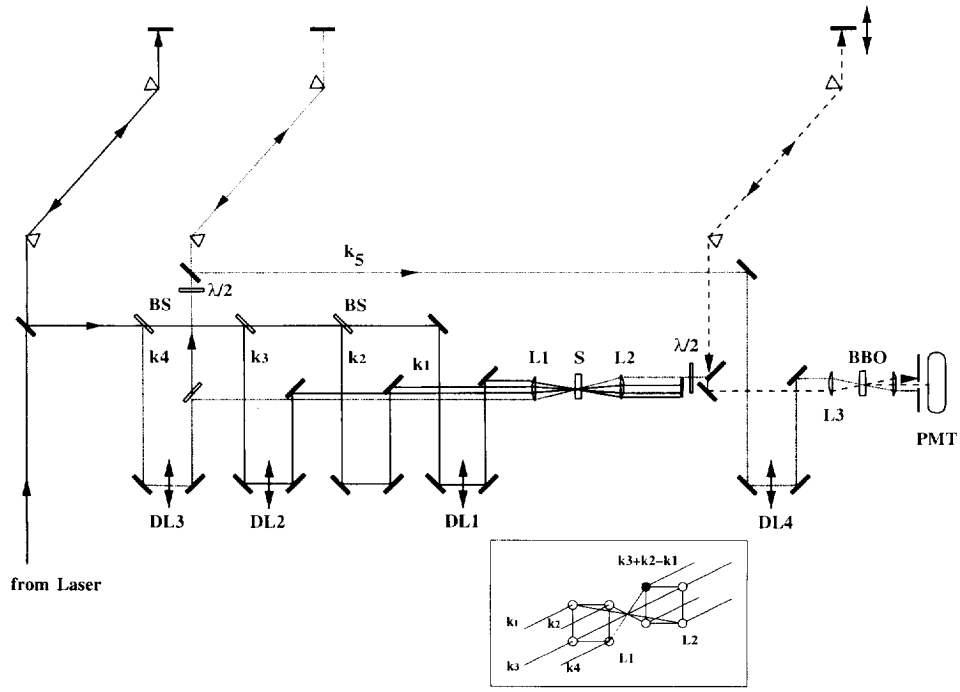

Fig. 2. Experimental apparatus: optical beams k_1 through k_4, scanning delay lines (DL1–DL4), focusing lenses (L1–L3), sample (S), photomultiplier detector (PMT), beamsplitters (BS). The k-vector geometry of the experiment is indicated in the inset. The Ti:sapphire laser is not shown.

tion of the OKE response with the optical dephasing spectral density is given elsewhere [29].

3. Experimental

The experimental setup consists of a femtosecond pulse Ti:sapphire laser, a five-beam experimental configuration and signal detection and processing electronics. The laser system has already been described in detail [21]. Briefly, a cw-argon-ion laser operating on all lines was used to pump a home-built Kerr-lens mode-locked Ti:sapphire laser of a standard design [30,31]. At 5 W of pump power and with a 3.5 mm crystal and 8% output coupler the Ti:sapphire laser routinely delivered a 84 MHz train of 12 to 15 fs duration pulses centered at 790 nm with 5–6 nJ pulse energies. Interferometric autocorrelations of the compensated pulses showed no evidence of chirp and the time-bandwidth product for sech^2 pulses was typically within 15% of the transform limited value.

The five-beam experimental scheme is illustrated in Fig. 2. Following prism-pair compensation for positive group velocity dispersion (GVD), which originates from the output coupler, several beamsplitters (BS) and a f = 60 mm achromatic doublet (L1), the pulse train was split into four beams of approximately equal intensity and with wavevectors k_1, k_2, k_3, and k_4 arranged in a boxcars geometry. The first three beams serve to generate the ordinary three-pulse photon-echo response in the momentum-matched direction $k_s = k_4 = k_3 + k_2 - k_1$. The fourth beam, k_4, hereafter denoted as the reference beam, is aligned collinear with the induced third-order polarization. All four beams are spatially and temporally overlapped at the position of the sample, a 150 μm thick free flowing jet of HDITCP in butanol or DMSO, and are recollimated with an identical 60 mm achromat (L2). The optical density of the sample is maintained at less than 0.3 at 790 nm. Pulse energies at the sample are about 0.5 nJ in each beam. The photon echo and the reference beam (k_4) are sent through a second set of fused silica prisms and finally refocused with a 60 mm achromatic doublet (L3) into a 150 μm thick type-I BBO crystal cut for second harmonic generation at

800 nm. The purpose of the second prism delay line is to compensate for positive GVD arising from L2 and L3.

The major part of the k_4 beam is split off before L1 to serve as the gating pulse, denoted as k_5 (see Fig. 2). This gating beam is sent through a third set of fused silica prisms to compensate for positive GVD of L3, and is spatially and temporally overlapped with the reference beam in the 150 μm BBO crystal. The k_4 beam serves as the zero-of-time reference for the up-conversion (i.e. gating) pulse, k_5, and as an alignment guide for echo gating. The reference beam is blocked during the photon echo measurements.

The cross-correlations of the pulses creating the third-order polarization in the sample, k_1 with k_2, k_3 and k_4, are measured with a 100 μm thick KDP crystal at the position of the sample. These cross-correlations are used to establish an absolute time origin for all of these beams. The instrument response is determined from the cross-correlation of the reference pulse with the gating pulse (k_R with k_5) measured with the same 150 μm BBO crystal that is used for up-conversion of the echo response. All beams are polarized parallel with respect to each other.

The intensity of the sum frequency of the photon echo and the gating pulse is detected in a background-free geometry with a photomuliplier (Hamamatsu 1P28) and amplified (Centronic PA-100). This signal is processed by a digital lock-in amplifier referenced to a chopper that modulated the gating beam (k_5) at a frequency of 500 Hz. The output of the lock-in amplifier is read and stored by a computer that simultaneously controlled three precision translation stages and thereby the relative timing of all beams at the position of the sample as well as at the time of arrival of the echo and gate pulse at position of the nonlinear crystal. Data are recorded at 2 fs intervals along the up-conversion time delay.

4. Results

4.1. Time-integrated photon echoes

Figs. 3a and 3b show the time-integrated photon echo signals obtained for HDITCP in both butanol and DMSO, respectively, detected in the $k_s = k_4 = k_3 + k_2 - k_1$ vector matching direction. In these cases

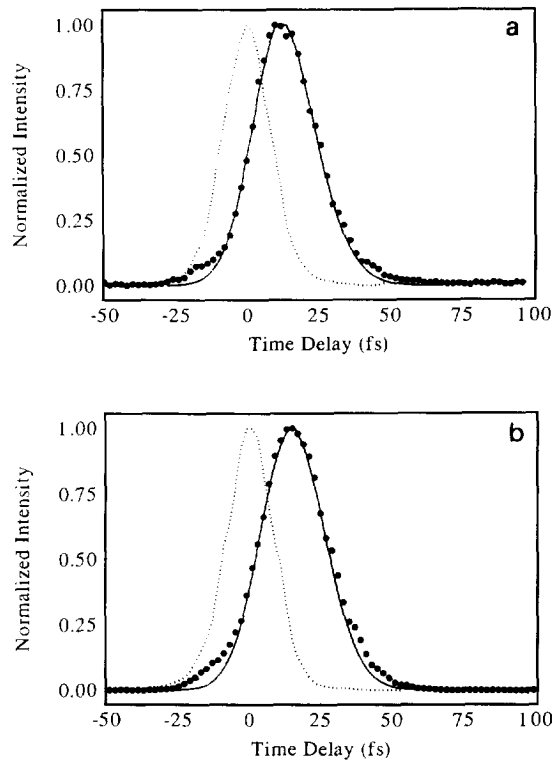

Fig. 3. (a) Measured time-integrated three-pulse photon echo signal of HDITC-perchlorate in DMSO. The $k_s = k_3 + k_2 - k_1$ signal is shown along with the second-order pump–probe cross-correlation. The line through the data points is the result of the spectral density simulation as described in the text. (b) Time-integrated photon echo signal of HDITCP in butanol. The solid line through the data points is the result of the spectral density simulation.

pulses 2 (k_2) and 3 (k_3) were simultaneously incident on the sample reducing the measured response to essentially the two-pulse photon echo case. As this plot shows, the echo signals as a function of τ are very similar for these two solvents. Fig. 3 also shows the cross-correlation of the grating forming beams, k_1 and k_2. This is the zero-of-time reference for the measurement. The time-integrated echo signals exhibit a time-shift and are broadened compared with the instrumental response reflecting the finite material response. The integrated signal for HDITCP in butanol peaks at a delay time of 14±2 fs whereas the signal collected for HDITCP in DMSO peaks at a delay time of 12±2 fs. The temporal shift is an important constraint in the choice of model parameters that are used in the simulation of the echo signals. Furthermore, the widths of the two time-integrated photon echo sig-

nals shown in Fig. 3 are almost identical, with butanol being slightly narrower. The small shoulder on the negative time portion of the time-integrated echo signals arises from a thermal grating contribution to the signal [21]. The thermal grating couples the $k_s' = k_3 - k_2 + k_1$ into the $k_s = k_3 + k_2 - k_1$ phase matching direction hence the direction of detection. Previous results obtained using the same solvents with HITCI, another cyanine dye, studied in a two-pulse geometry and with somewhat longer duration pulses yielded slightly larger time shifts [21]. The echo widths for HITCI were very similar to each other in these two solvents but broader than those observed here.

4.2. Solvent spectral density and simulation

The approach described in Section 2 for the simulation of the three-pulse echo signal of the cyanine dyes makes explicit use of the spectrum of solvent fluctuations. This spectrum is taken from measurements of the optical heterodyne-detected OKE response of each solvent. This measurement represents the molecular polarizability correlation function, $\langle[\alpha_{ij}(0), \alpha_{kl}(t)]\rangle$, and, by the fluctuation–dissipation theorem, the associated equilibrium fluctuations of the pure liquid. The anisotropic part of the polarizability spectral density of neat DMSO is generated from the experimental optical Kerr effect susceptibility according to Eq. (3).

The solid lines superimposed on the experimental data for HDITCP in butanol and DMSO in Figs. 3a and 3b are the results of the simulation of the time-integrated three-pulse photon echo signal in these solvents. The simulations employ the polarizability spectral density for butanol and for DMSO (not shown) and measured pulse durations. These polarizability spectral densities are connected with the spectral density for electronic energy fluctuations (i.e. the optical dephasing spectral density) [29]. The only adjustable parameter in the simulation is the magnitude of the solute–solvent coupling, N, given in Eq. (3). The excellent agreement with experiment suggests that the simulation accurately determines the time-shift and the width of the time-integrated photon echo. This procedure obtains values for the coupling parameter, N, of 4 and 2 for butanol and DMSO, respectively. The polarizabilities of these two solvents are almost the same although a larger frequency range of solvent fluctuations is used for DMSO (0–730 cm^{-1}) than for butanol (0–500 cm^{-1}). Additional details of the simulation are discussed in Ref. [29].

4.3. Time-gated photon echoes

The time-gated photon echo responses for HDITCP in DMSO are shown in Fig. 4. The data have been plotted in a series of panels to give a sense of the evolution of the polarization response. (Note that the value of the ordinate changes from panel to panel.) Fig. 4a shows the associated $k_4 - k_5$ cross-correlation centered at $t' = t_{3g} = 0$. The measurements were performed by scanning the t' gate-pulse delay with 2 fs steps for various values of the pulse separation τ (i.e. time between the k_1 and k_2 pulses). These waveforms are characterized by three parameters: (i) the magnitude of the polarization maximum following the k_3

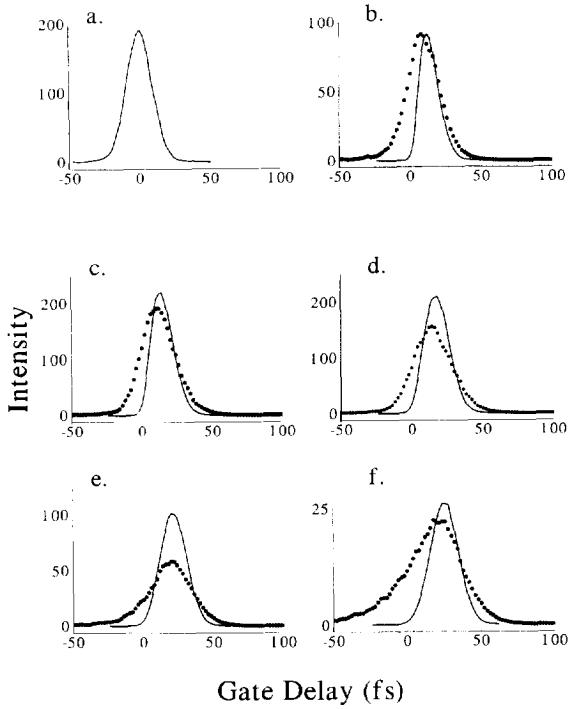

Fig. 4. Comparison of measured and calculated time-gated three-pulse echo signals of HDITCP in DMSO. The time axis is the t' time-gating coordinate. Each panel is for a different value of τ: (a) autocorrelation only; (b) $\tau = 0$ fs; (c) $\tau = 10$ fs; (d) $\tau = 20$ fs; (e) $\tau = 30$ fs; (f) $\tau = 40$ fs. The points are the experimental data and the solid lines are the simulated responses. Notice the changes in the intensity axis for each panel.

pulse; (ii) the width of the response at each delay; and (iii) the temporal shift of the polarization maximum with respect to $t' = 0$. The modulus square of the echo field is largest for grating forming pulse time delays of $\tau = 12$ to 15 fs while having attained less than half of this maximum intensity for zero delay. The polarization signal is less than the maximum value for τ less than the pulse duration because of convolution effects; the time-gated signal has a maximum at $t' \approx$ pulse fwhm. The signal is seen to decay to 10% of the maximal value for delay times of $\tau = 40$ fs, thereafter quickly approaching zero without recurrence. The rapid decrease in signal level is consistent with the time-integrated photon echoes presented in Fig. 3a. The integrated intensity of the time-gated signals agrees with time-integrated echo signal at the corresponding time delay. Finally, the width of the time-gated polarization response increases significantly with increasing values of τ.

The most pronounced characteristics of the time-gated signals in Fig. 4 is the temporal shift from the zero-of-time ($t' = 0$) as well as the broadening of the response for increasing grating-pulse delays. As expected, the temporal shift increases with grating-pulse separation as a result of the increased time required for polarization rephasing. For delays such that the echo forming pulses are well separated, the time-gated response always attains its maximum value at $t' < \tau$; the maximum never appears at $t' = \tau$ as expected in the so-called large inhomogeneous broadening limit. Fig. 5 shows the temporal shift of the modulus-square

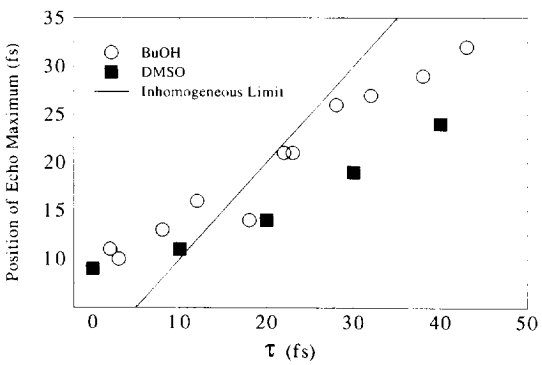

Fig. 5. Position of the polarization maximum (t'_{max}) for different grating pulse delays (τ). The squares are data points for HDITCP in DMSO and the filled circles are for HDITCP in butanol. The diagonal line refers to the position of the maximum expected for the Markovian timescale separated limit.

of the echo field as a function of delay τ for HDITCP in butanol and DMSO. This plot shows a significant deviation from the $t' = \tau$ case, which is indicated by the solid line above the points for butanol and DMSO. Some of the deviation results from the finite duration of the k_1, k_2 and k_3 pulses, but the slopes of the experimental curves differ significantly from the $t' = \tau$ value. Furthermore, there is a clear difference between the time-shifts for the two chromophore–solvent systems. This last result is in contrast to the almost identical time-integrated photon echo signals presented above.

4.4. Simulation of time-gated echoes

The measured time-gated photon echoes are simulated given knowledge of the spectral density of solvent nuclear motions and the coupling mechanism between solvent and solute. The approach taken here is reflected in Eqs. (2)–(5) where the measured solvent OKE susceptibility is used to obtain $C(\omega)$. These simulations for HDITCP in DMSO are the solid lines in Figs. 4b–4f. The simulated signals are also plotted in 2 fs increments along the time gating axis, t'. The signals are calculated using the solute–solvent coupling parameter, N, obtained from fitting the time-integrated photon echo for DMSO in Fig. 3. The simulated time-gated signals are normalized to the $\tau = 0$ fs experimental value; the relative intensities of the simulated time-gated echoes are in reasonably good agreement with the experimental results with the most significant deviation at $\tau = 30$ fs (Fig. 4e). The temporal shifts are not matched at any value so the absolute simulated shifts all agree with the experimental values within the experimental margin of error; the experimental zero-of-time was obtained via $k_4 - k_5$ cross-correlation as described above. No other 'arbitrary' time-shift has been introduced in the experimental/simulation comparison! The measured signals are, however, always broader than the simulated signals. The comparison of experimental and simulated responses for HDITCP in butanol are the same: different experimental and simulated intensities at small values of t', very good agreement for the time shifts but consistently narrower experimental time-gated echo widths. These results are not shown here for the sake of brevity.

Three contributions to the total polarization response not included in the model may account for the discrepancy: (i) chromophore intramolecular modes

that result in additional vibronic transitions contributing to the optical excitation and the optical coherence; (ii) a frequency-dependent coupling, $N(\omega)$, in the spectral density and; (iii) a thermal grating contribution to the signal. These topics will be discussed in the Section 5.

5. Discussion

The direct measurement of time-gated photon echo responses of a chromophore in solutions of DMSO and butanol is the principle result of this study. Comparison of the measured and simulated time-gated third-order polarization responses, the latter obtained using the measured solvent OKE susceptibility, have also been made. This method for calculating photon echo signals assumes that the spectrum of equilibrium fluctuations of the pure liquid determine the spectrum of modulations of the optical transition frequency resulting in optical dephasing. The bath fluctuations were introduced in the echo calculations using measured solvent spectral densities. Two conclusions result from the analysis of the cyanine dye chromophore response in a range of solvents. The first is that the simulations performed without consideration of vibronic structure or a frequency-dependent coupling are in very good agreement with time-integrated photon echo signals but do not fully reproduce the measured time-gated polarization responses. The second point is that the richness in the various time-gated polarization signals shown in Fig. 4 gives much more information about the nature of the spectral density for electronic energy fluctuations.

The conventional two-pulse photon echo is a measure of the integrated third-order polarization shown as the shaded area in Fig. 1a. In time-gated photon echo spectroscopy the instantaneous value of the polarization reponse, hence the echo shape itself rather than its integral, is detected as a function of time delay between the two pulses; cf. Fig. 1b. The time-gated polarization experiment in a two (or three) pulse geometry employs a sequence of three (or four) pulses and becomes two-dimensional. The first two (or three) pulses create the third-order polarization via degenerate four wave mixing in the material and the third (or fourth) pulse samples the time-dependent variation of the echo intensity for a given separation of the polarization forming pulses.

In the case of separable timescales, solvent-induced chromophore dephasing in the Markovian limit, the *echo shape* can be expressed as a product of a homogeneous contribution $H(t)$ and an inhomogeneous contribution $I(t)$ convoluted with an instrument response function (here assumed to be a delta-function), that is

$$S(\tau, t) \propto H(t' + \tau) I(t' - \tau). \tag{6}$$

In the Markovian description the inhomogeneous contribution to the polarization response is characterized by a Gaussian broadening function and the homogeneous contribution as an exponential decay of the optical coherence (i.e beginning at the time of the first pulse). Ensemble rephasing and echo formation can occur as a result of inhomogeneous broadening. The resulting Gaussian polarization response is centered at time $t' = \tau$ reflecting maximal ensemble rephasing and will not change in amplitude for different values of τ[4]. The homogeneous component, on the other hand, is purely dissipative. The result is that the maximum of the echo profile is peaked at $t' < \tau$. Furthermore, in the presence of homogeneous broadening, the polarization will decay along the $t' = \tau$ diagonal. Therefore, the diagonal measurement (i.e. $t' = \tau$) would give the homogeneous dephasing time while an 'orthogonal' measurement ($t' + \tau$ = constant) would yield the inhomogeneous broadening.

In liquids the chromophore/bath response can no longer obeys the well-separated timescales condition. Rather, the bath responds on a range of timescales that we propose occurs, at least to first-order, according to the spectrum of fluctuations of the pure liquid. Simple decay (i.e. exponential) and broadening (i.e. Gaussian) functions will no longer describe the temporal behavior of the polarization response; the diagonal measurement will give a complicated decay profile. Furthermore, polarization preparation with real (i.e. finite duration) pulses will introduce additional time shifts of the signal maxima for times comparable to the pulse durations. The finite pulse 'convolution' would manifest itself as a delay in the t' value at which the echo profile reaches a maximum. For values of τ larger than the pulse durations, however, the slope of

[4] There is always a dissipative path coupled to the optically prepared coherence; that is, radiative decay. Here, this is essentially infinitely long (>1 ns for this chromophore).

the plot of time of the polarization maximum t'_{max} versus τ would be equal to one for the timescale separated case but less than one for the non-Markovian case. Fig. 5 shows the experimental deviations from behavior expected for inhomogeneous broadening. The slope of the deviation of the polarization maximum from $t' = \tau$ reflects the non-Markovian broadening in the system. The different slopes for the time-shift data in Fig. 5 reflect the differences in the actual optical dephasing spectral densities.

As shown in Fig. 4, the time shifts of the calculated up-converted photon echo signals are found to agree very well with the measured signals. The disagreement in the width of the time-gated echo responses indicates that either: (1) the solvent coupling parameter is frequency-dependent, i.e. $N \rightarrow N(\omega)$; (2) the vibronic structure of the chromophore must be considered in the simulation; and (3) a small thermal contribution contributes to the gated echo signal at the zero-of-time. In either case, the time-gated echo has already demonstrated itself to be a more sensitive probe of the solvent fluctuations than the time-integrated signal.

In the case of the time-integrated echo signal, the solute–solvent coupling parameter, N, is the only adjustable parameter for 'fitting' the simulation to the data. The spectrum of fluctuations, which is a generalization of the inverse bath correlation time in the MBO picture, is here equated to the polarizability spectral density of pure solvent. This results in an overdetermined fitting problem with one fitting parameter and two constraints; the time shift and the echo width. The analysis is overdetermined within the assumption to omit additional optical transitions that must actually contribute to the prepared coherence. The parameter that accounts for the interaction between solute and solvent, N in Eq. (4), is here assumed to be frequency independent. In general, the measured OKE-spectral density is not necessarily the spectral density for optical dephasing. Therefore, the correction to obtain the dephasing spectral density could be achieved by making the coupling frequency-dependent, i.e. $N \rightarrow N(\omega)$. Then the analysis for time-integrated echoes would no longer be unique. Incorporation of $N(\omega)$ amounts to finding the appropriate spectral density for the observed process. The frequency-dependent coupling could be determined by least-squares minimization in fitting but this would not yield a unique solution. By contrast, the greater amount of information obtained from the time-gated polarization response measurements $N(\omega)$ could be established more uniquely. From preliminary simulation results we have found that different forms for $N(\omega)$ yield better agreement between the widths and amplitudes of the simulated and experimental results shown in Fig. 4.

The assumption of omitting the additional vibronic transitions is also an important consideration at this stage. The equilibrium spectral density serves as a useful reference point from which to establish the frequency dependence of the coupling of the solvent fluctuations to the optical transition moment. We have undertaken multi-mode simulations of three-pulse time-integrated photon echo and time-gated polarization response measurements in the solvents used in the present experiments and for two cyanine dye chromophores: HITCI and HDITCP. The vibronic structure and vibrational mode displacements were obtained by simulataneously simulating the pump–probe signal, integrated three-pulse signal and the measured absorption spectrum. The parameters for the intra-chromophore modes and the spectral density were then used to simulate the time-gated polarization response. This more comprehensive and complete simulation results in broadened time-gated echo shapes that more closely agree with experiment. These results along with more extensive experimental measurements will be presented elsewhere [32].

Finally, a small thermal contribution to the total polarization response as seen in the time-integrated echoes would give a contribution to the time-gated polarization response about the zero-of-time. Preliminary results using a cavity-dumped Ti:sapphire oscillator where the lower repetition rate and average power precludes the creation of a thermal grating indeed show a reduction in the zero-of-time response. The longer delay time polarization response is still not in complete agreement with experiment implying that the aforementioned factors (frequency-dependent coupling and additional vibronic transitions) need to be included.

6. Conclusions

We have demonstrated the idea that time-gated detection of the third-order polarization response, i.e.

photon echo, of chromophores in solution is a measurement that is very sensitive to spectrum of bath fluctuations that affect optical dephasing. The scheme involves gated detection of the echo, which allows direct detection of the asymmetry in the echo shape. In the limit of timescale separation of the bath fluctuations, the asymmetry reflects the product of inhomogeneous (i.e. symmetric Gaussian) and homogeneous (i.e. exponentially decaying) contributions to the nonlinear response function. Another advantage of the time-gated measurements involves replacing the integration in Eq. (1) with a simple and finite convolution over the gate pulse duration. These measurements have been performed and indeed reflect greater sensitivity to the form of the spectral density; the multidimensional data allow determining a frequency-dependent coupling parameter.

Time-integrated two- and three-pulse photon echo signals are well simulated using the solvent polarizability spectral density and a frequency-independent coupling parameter. This indicates that the solvent spectral density obtained from impulsive OKE measurements essentially accounts for the solvent fluctuations that dictate the evolution of optical coherence of HDITCIP in polar solvents. The disagreement between the model simulations and *the time-gated experimental results indicate that frequency-dependent couplings and inclusion of chromophore vibrational modes* must be taken into account.

This approach is now being applied to the further evaluation of $N(\omega)$ in these cyanine dye chromophore solutions, charge-transfer reactions and fluctuations that occur in proteins.

Acknowledgement

We thank Professor James Skinner and Professor Richard Stratt for helpful comments and the referee for an important suggestion. We acknowledge the financial support of the National Science Foundation (NSF-NYI), University of Pennsylvania Materials Laboratory (NSF-DMR), the ACS Petroleum Research Fund (type G), Deutsche Forschungsgemeinschaft, and the Department of Education (GAANN). NFS is the recipient of a David and Lucile Packard Foundation fellowship and is an Arnold and Mabel Beckman Young Investigator.

Note added

While this Letter was under review we became aware of a similar study of time-resolved photon echoes in ethylene glycol by Wiersma and co-workers [33]. Their experiments were performed in a two-pulse photon echo geometry while we employ a more general three-pulse geometry. Also, they do not establish the zero-of-time for the polarization response and actually determine this important parameter by simulation and fitting of the signal using a non-Markovian MBO model. Their finding that the solvent response is non-Markovian is the same conclusion that we reach here and in Ref. [21].

References

[1] T.-S. Yang and A.B. Myers, J. Chem. Phys. 100 (1994) 8573.
[2] G.R. Fleming and P. Hänggi, eds., Activated barrier crossing (World Scientific, Singapore, 1993).
[3] J.T. Hynes, Ann. Rev. Phys. Chem. 36 (1985) 573.
[4] D. Chandler, J. Stat. Phys. 42 (1986) 49.
[5] G.R. Haynes and G.A. Voth, J. Chem. Phys. 99 (1993) 8005.
[6] S. Mukamel, Ann. Rev. Phys. Chem. 41 (1990) 647; Advan. Chem. Phys. 70 (1988) 165.
[7] N.E. Shemetulskis and R.F. Loring, J. Chem. Phys. 97 (1992) 1217, and references therein.
[8] H.C. Meijers and D.A. Wiersma, J. Chem. Phys. 101 (1994) 6927.
[9] Y.S. Bai and M.D. Fayer, Chem. Phys. 128 (1988) 135.
[10] S. Mukamel and R.F. Loring, J. Opt. Soc. Am. B 3 (1986) 595.
[11] Y.J. Yan and S. Mukamel, Phys. Rev. A 41 (1990) 6485; J. Chem. Phys. 94 (1991) 179.
[12] W.B. Bosma, Y. Yan and S. Mukamel, Phys. Rev. A 42 (1990) 6920.
[13] C.H. Wang, Spectroscopy of condensed media (Academic Press, New York, 1985).
[14] A.M. Weiner, S. De Silvestri and E.P. Ippen, J. Opt. Soc. Am B 2 (1985) 654.
[15] J.-Y. Bigot, M.T. Portella, R.W. Schoenlein, C.J. Bardeen, A. Migus and C.V. Shank, Phys. Rev. Letters 66 (1991) 1138.
[16] E.J. Nibbering, D.A. Wiersma and K. Duppen, Phys. Rev. Letters 66 (1991) 2464.
[17] T. Joo and A.C. Albrecht, Chem. Phys. 176 (1993) 233.
[18] P. Cong, Y.J. Yan, H. Deuel and J.D. Simon, J. Chem. Phys. 100 (1994) 7855;
P. Cong, H.P. Deuel and J.D. Simon, Chem. Phys. Letters 212 (1993) 367.
[19] W.P. de Boeij, M.S. Pshenichnikov, K. Duppen and D.A. Wiersma, Chem. Phys. Letters 224 (1994) 243.
[20] C. Bardeen and C.V. Shank, Chem. Phys. Letters 226 (1994) 310.

[21] P. Vöhringer, D.C. Arnett, R.A. Westervelt, M.J. Feldstein and N.F. Scherer, J. Chem. Phys. (1995) 102, March 8 issue.
[22] D.C. Arnett, P. Vöhringer, R.A. Westervelt, M.J. Feldstein and N.F. Scherer, Springer series in chemical physics, Vol. 60. Ultrafast phenomena IX, ed. P. Barbara (Springer, Berlin, 1994) p. 482.
[23] M. Cho and G.R. Fleming, J. Phys. Chem. 98 (1994) 3478.
[24] H. Mahr and M.D. Hirsch, Opt. Commun. 13 (1975) 96.
[25] M.D. Fayer, in: Spectroscopy and excitation dynamics of condensed molecular systems, eds. V.M. Agronovitch and R.M. Hochstrasser (North-Holland, Amsterdam, 1983) p. 185.
[26] P. Leisching, T. Dekorsy, C. Waschke, H. Roskos, K. Leo, H. Kurz and K. Köhler, Springer series in chemical physics, Vol. 60. Ultrafast phenomena IX, ed. P. Barbara (Springer, Berlin, 1994) p. 337.
[27] M. Koch, F. Jahnke, T. Meier, J. Feldmann, W. Schäfer, P. Thomas, S.W. Koch, E.O. Göbel and H. Nickel, Springer series in chemical physics, Vol. 60. Ultrafast phenomena IX, ed. P. Barbara (Springer, Berlin, 1994) p. 354.
[28] R.J.D. Miller, J. Deak, S. Palese, M. Pereira, L. Schilling, Springer series in chemical physics, Ultrafast phenomena VIII, (Springer, Berlin, 1993) p. 525.
[29] T.-S. Yang, P. Vöhringer, D.C. Arnett and N.F. Scherer, in preparation.
[30] M.T. Asaki, C.P. Huang, D. Garvey, J. Zhou, H.C. Kapteyn and M.M. Murnane, Opt. Letters 18 (1993) 977.
[31] F. Krausz, Ch. Spielmann, T. Brabec, E. Wintner and A.J. Schmidt, Opt. Letters 17 (1992) 204.
[32] T.-S. Yang, D.C. Arnett, P. Vöhringer and N.F. Scherer, in preparation.
[33] M.S. Pshenichnikov, K. Duppen and D.A. Wiersma, Phys. Rev. Letters 74 (1995) 674.